AD-A075 213 NAVAL POSTGRADUATE SCHOOL MONTEREY CA F/G 4/2
DETERMINATION OF VERTICAL WIND SHEAR FROM LINEAR COMBINATIONS O--ETC(U)
SEP 79 H E FLEMIN
UNCLASSIFIED NPS63-79-004 NL

1 OF 1
AD
AD75213

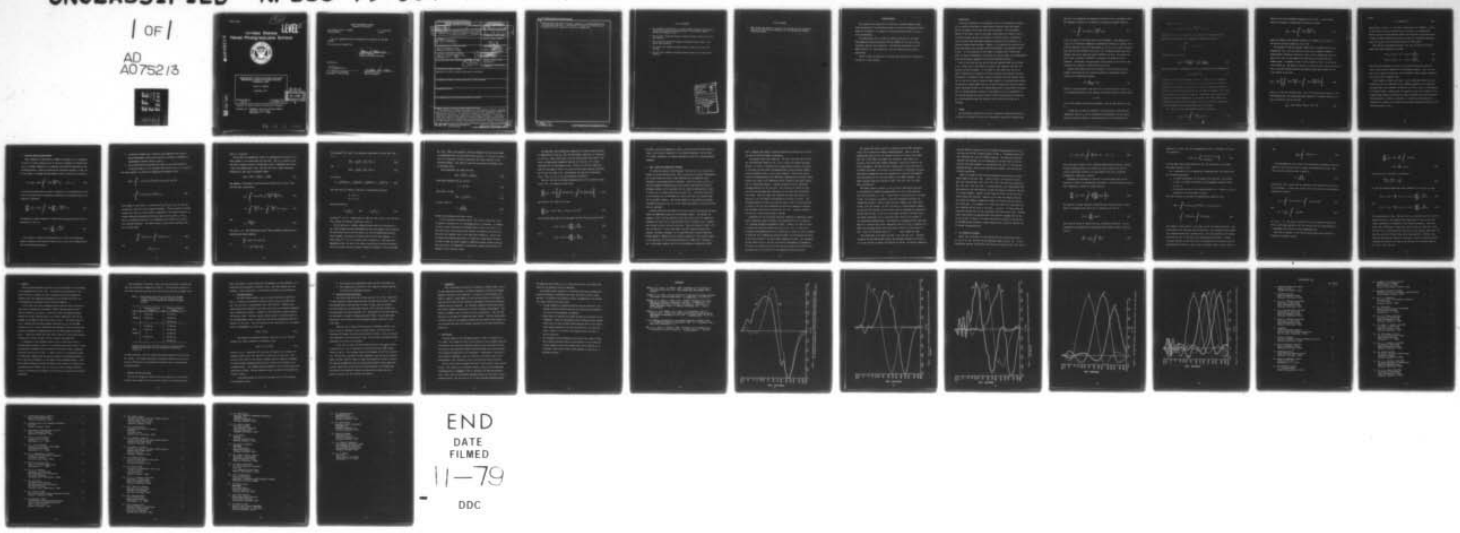

END
DATE FILMED
11-79
DDC

NPS63-79-004

LEVEL II

AD A075213

United States Naval Postgraduate School

DETERMINATION OF VERTICAL WIND SHEAR FROM LINEAR COMBINATIONS OF SATELLITE RADIANCE GRADIENTS: A THEORETICAL STUDY

Henry E. Fleming

September 1979

Technical Report Period: 1 October 1978 – 22 September 1979

Approved for public release; distribution unlimited.

Prepared for: Commander, Naval Air Systems Command,
Department of the Navy
Washington, D. C. 20361

NAVAL POSTGRADUATE SCHOOL
Monterey, California

Rear Admiral Tyler F. Dedman
Superintendent

J. R. Borsting
Provost

The work reported herein was supported by the Naval Air Systems Command.

This report was prepared by:

Henry E. Fleming
Adjunct Research Professor

Reviewed by:

G. J. Haltiner, Chairman
Department of Meteorology

William M. Tolles
Dean of Research

SECURITY CLASSIFICATION OF THIS PAGE *(When Data Entered)*

REPORT DOCUMENTATION PAGE

READ INSTRUCTIONS BEFORE COMPLETING FORM

1. REPORT NUMBER: NPS63-79-004	2. GOVT ACCESSION NO.
3. RECIPIENT'S CATALOG NUMBER: Technical rept.	
4. TITLE (and Subtitle): Determination of Vertical Wind Shear from Linear Combinations of Satellite Radiance Gradients: A Theoretical Study.	5. TYPE OF REPORT & PERIOD COVERED: 1 Oct 78-22 Sep 79
	6. PERFORMING ORG. REPORT NUMBER
7. AUTHOR(s): Henry E. Fleming	8. CONTRACT OR GRANT NUMBER(s): 16
9. PERFORMING ORGANIZATION NAME AND ADDRESS: Naval Postgraduate School, Monterey, California 93940	10. PROGRAM ELEMENT, PROJECT, TASK AREA & WORK UNIT NUMBERS: N00019-79-WR91115 MB PE
11. CONTROLLING OFFICE NAME AND ADDRESS: Naval Air Systems Command, 370G, Washington, D. C. 20361	12. REPORT DATE: Sep 1979
	13. NUMBER OF PAGES: 44
14. MONITORING AGENCY NAME & ADDRESS *(if different from Controlling Office)*	15. SECURITY CLASS. *(of this report)*: Unclassified
	15a. DECLASSIFICATION/DOWNGRADING SCHEDULE

16. DISTRIBUTION STATEMENT *(of this Report)*

Approved for public release; distribution unlimited.

17. DISTRIBUTION STATEMENT *(of the abstract entered in Block 20, if different from Report)*

18. SUPPLEMENTARY NOTES

19. KEY WORDS *(Continue on reverse side if necessary and identify by block number)*

20. ABSTRACT *(Continue on reverse side if necessary and identify by block number)*

By applying the thermal wind equation to the radiative transfer equation, one can derive the vertical wind shear from horizontal gradients of radiances measured by satellite. The vertical resolution of the wind shear can be optimized by using linear combinations of radiance gradients. A theoretical study was conducted to determine the optimal pressure intervals over which wind shears could be resolved when using weighting functions associated with the SSH sounder of the Defense Meteorological Satellite Program, and those → next page

associated with the TOVS instrument package on the TIROS-N/NOAA series of operational satellites. Two distinct computational approaches are presented and their respective results are summarized.

LIST OF FIGURES

1. The normalized derivative of a single kernel function (solid curve) versus the normalized averaging kernel of four kernel function derivatives (dashed curve).

2. The two best normalized bimodal averaging kernels based on the four SSH channels.

3. The three best normalized bimodal averaging kernels based on the eleven TOVS channels.

4. The three best unimodal averaging kernels based on the four SSH channels.

5. The five best unimodal averaging kernels based on the eleven TOVS channels.

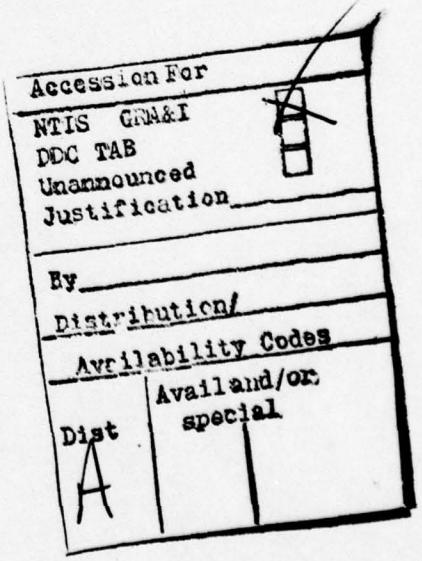

LIST OF TABLES

1. Best layers over which to calculate the average vertical wind shear, based on the SSH and TOVS sounders, for the bimodal and unimodal averaging kernels.

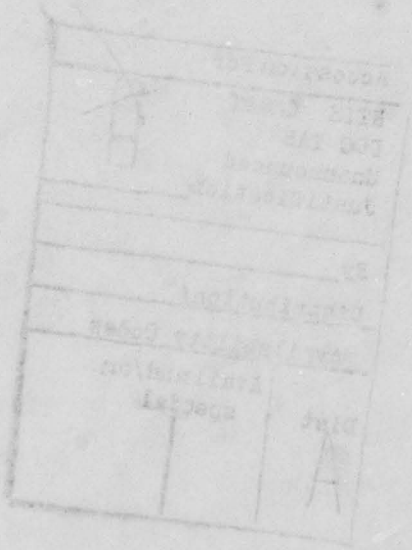

ACKNOWLEDGMENTS

This research was supported by the Naval Air Systems Command through their sponsorship of the Meteorology Chair at the Naval Postgraduate School, Monterey, California. The support of Professor George Haltiner is gratefully acknowledged.

The author would like to thank the officers and staff of the Naval Environmental Prediction Research Facility (NEPRF) for the use of their facilities and for their assistance. The detailed discussions with the NEPRF Director, Dr. Allen Weinstein, were very helpful and are greatly appreciated.

Special thanks are extended to Professor Hans Panofsky for introducing the author to this problem.

1. INTRODUCTION

If the wind components at one pressure level of the atmosphere are given and the vertical wind shear is known between the given level and another level, the winds at the second level can be inferred. Over data-sparse regions of the earth, such as the oceans, winds usually are known at only a few levels because the data are limited to aircraft reports, cloud motion vectors derived from time-lapse sequences of satellite cloud pictures, or constant pressure-level balloons. However, if in addition the vertical wind shear were known, then the winds could be determined at intermediate levels as well. It is the purpose of this report to examine from a theoretical point of view the possibility of deriving the vertical shear of the geostrophic wind from horizontal gradients of satellite-measured radiances.

Work of this kind has been done by Zak and Panofsky (1968) and by Grody, et al. (1979), but in both papers the authors used radiances from only one spectral interval (channel). *It is shown in this report* that the use of linear combinations of radiances from many channels yields greater accuracy. Furthermore, an extensive study is made to determine the best pressure intervals to use for the Special Sensor-H (SSH) sounder of the Defense Meteorological Satellite Program (DMSP) and for the Tiros-N Operational Vertical Sounder (TOVS) instrument package on the TIROS-N/NOAA series of operational satellites. Once the optimum pressure interval is determined, one of the boundaries of the interval becomes the pressure level at which the winds must be known and the other boundary becomes the pressure level at which the winds can be inferred.

2. THEORY

The relationship between the vertical atmospheric temperature profile as a function of pressure T(p) and the corresponding radiance R_ν emerging from

the top of the atmosphere and measured by satellite over a wavenumber interval (channel) centered at ν is given by the radiative transfer equation

$$R_\nu = \int_{p_T}^{p_s} B_\nu [T(p)] [-\frac{d\tau_\nu(p)}{dp}] dp. \quad (1)$$

In Eq. (1) $B_\nu(T)$ is the Planck function at wavenumber ν and temperature T, $\tau_\nu(p)$ is the fractional atmospheric transmittance between the pressure level p and the effective top of the atmosphere p_T, and p_s is the surface pressure. Note that the usual boundary term in Eq. (1) is missing because only those channels that do not sense the ground radiation are used. The reason for this is that it would be difficult to interpret the gradient of such radiances. Furthermore, the geostrophic wind equation is not valid in the boundary layer because of surface frictional forces.

Another relationship that will be needed is the one between the geostrophic wind shear and the horizontal gradient of temperature which is given by the thermal-wind equation

$$\alpha \vec{k} \times \frac{\partial \vec{V}}{\partial(\ell n p)} = \nabla_p T, \quad (2)$$

where $\vec{V}$ is the geostrophic wind vector, $\vec{k}$ is the vertical unit vector, ∇_p is the gradient operator on the surface of constant pressure, and the scalar

$$\alpha = f/R$$

is the ratio between the coriolis parameter f and the gas constant for air R.

To make Eqs. (1) and (2) compatible, one can choose a fixed vertical temperature profile T_o that is sufficiently representative of the area to which the gradient operator is being applied that the following Taylor

approximation is valid:

$$B_\nu(T) = B_\nu(T_o) + \frac{dB_\nu(T_o)}{dT}(T - T_o). \tag{4}$$

Therefore, if Eq. (4) is applied to Eq. (1) and the isobaric gradient operator ∇_p is applied to the resulting equation, one obtains

$$\nabla_p R_\nu = \int_{t_T}^{t_s} \nabla_p T(t)\, K_\nu(t)\, dt, \tag{5}$$

where the kernel function

$$K_\nu(t) = \frac{dB_\nu[T_o(t)]}{dT(t)} \frac{d\tau_\nu(t)}{dt} \frac{dt}{d(\ell np)}, \tag{6}$$

and the variable of integration p has been replaced by the transformation

$$t = a\, p^{2/7} + b \tag{7}$$

in which a and b are appropriate constants. (The purpose in making the transformation (7) is to distribute the kernel functions more uniformly throughout the vertical extent of the atmosphere, since they determine the levels of the atmosphere from which the radiation is emitted.) The limits of integration t_s and t_T in (5) are the transformed surface pressure and effective top of the atmosphere, respectively. Note that terms in (4) involving T_o vanish when the gradient operator is applied to them because they are constant over the horizontal space coordinates.

Eqs. (2) and (5) are now related through $\nabla_p T$, that is,

$$\nabla_p R_\nu = \alpha \vec{k} \times \int_{t_T}^{t_s} \frac{\partial \vec{V}}{\partial t} K_\nu(t)\, dt, \tag{8}$$

which is one of the fundamental equations we will need. A second basic result is obtained by integrating (8) by parts to obtain

$$\nabla_p R_\nu = -\alpha \vec{k} \times \int_{t_T}^{t_s} \vec{V}(t) \frac{dK_\nu(t)}{dt} dt, \qquad (9)$$

where the boundary term vanishes because $K_\nu(t)$ vanishes at t_s and at t_T. One now can work with either Eq. (8) or (9).

The approach of Zak and Panofsky (1968) will be followed first by considering Eq. (9). Since the kernel function $K_\nu(t)$ somewhat resembles a normal density probability function in that it has a single peak value and falls off to zero on each side of its peak value, its derivative has a bimodal shape. An example of such a curve is given in Fig. 1 by the solid curve labeled D_1. The shape of curve D_1 is typical of the function $dK_\nu(t)/dt$ in that it has well defined positive and negative modes which permit Eq. (9) to be written in the form

$$\nabla_p R_\nu = -\alpha \vec{k} \times \left\{ \int_{t_T}^{t_c} \vec{V}(t) \frac{dK_\nu(t)}{dt} dt - \int_{t_c}^{t_s} \vec{V}(t) \left| \frac{dK_\nu(t)}{dt} \right| dt \right\}, \qquad (10)$$

where t_c is the zero-crossing level. Since the differentiated kernels in (10) are both positive, the second mean-value theorem for integrals applies, and one can write Eq. (10) in the form

$$\Delta_p R_\nu = \beta \vec{k} \times [\vec{V}(t_1) - \vec{V}(t_2)] = \beta \vec{k} \times \delta \vec{V}, \qquad (11)$$

where

$$\beta = [-\alpha K_\nu(t_c)]^{-1} , \tag{12}$$

since $K_\nu(t_s) = K_\nu(t_T) = 0$. All that is known about the arguments t_1 and t_2 is that they are in the intervals $[t_T, t_c]$ and $[t_c, t_s]$, respectively. However, since the differentiated kernel functions have well-defined peaks in each of these intervals (see curve D_1 in Fig. 1), reasonable approximations for t_1 and t_2 are the pressure levels of these peaks.

Since $\delta\vec{V}$ can be determined from Eq. (11), one can write the required geostrophic wind components as follows:

$$u(t_1) = u(t_2) + \delta u = u(t_2) + \beta\left(\frac{\partial R_\nu}{\partial y}\right)_p \tag{13}$$

$$v(t_1) = v(t_2) + \delta v = v(t_2) - \beta\left(\frac{\partial R_\nu}{\partial x}\right)_p , \tag{14}$$

where the wind components at level t_1 are inferred from those given at level t_2 and from the components of the radiance gradient. Eqs. (13) and (14) are the results obtained by Zak and Panofsky (1963); however something more can be done to improve them.

The two modes of curve D_1 in Fig. 1 are so broad that there is a high probability that the components of the radiance gradient do not represent the geostrophic wind component differences at levels t_1 and t_2 as determined by the peak values. Clearly, what is required is that the two modes of the bimodal kernel function derivative be made to approach Dirac delta functions (distributions) as clearly as possible. A method for achieving this is provided by a variant of the Backus-Gilbert method (Backus and Gilbert, 1970). (Also see Conrath, 1972.)

3. MODIFIED BACKUS-GILBERT METHOD

Since radiances are measured in a number of channels, it is reasonable to use all of those radiances that do not have a component of ground radiation in a linear combination to accomplish the objectives described in the preceding section. Begin by replacing the continuous variable ν in Eq. (9) by the index i to signify the ith channel, that is, write (9) in the form

$$\vec{r}_i = \nabla_p R_i = -\alpha\vec{k} \times \int_{t_T}^{t_s} \vec{V}(t) \frac{dK_i(t)}{dt}\, dt, \qquad i=1,\ldots,n. \tag{15}$$

If one now multiplies each of these n equations by a yet-unspecified coefficient c_i and then sums the resulting n equations, the following linear combination is obtained:

$$\sum_{i=1}^{n} c_i \vec{r}_i = -\alpha\vec{k} \times \int_{t_T}^{t_s} \vec{V}(t)\left[\sum_{i=1}^{n} c_i \frac{dK_i(t)}{dt}\right] dt. \tag{16}$$

The quantity in square brackets is called the averaging kernel and will be denoted by D, that is,

$$D(\vec{c},t) = \sum_{i=1}^{n} c_i \frac{dK_i(t)}{dt}. \tag{17}$$

One is free to choose the coefficients c_i of (16) in any reasonable manner; therefore, they should be chosen so as to give the averaging kernel (17) the following properties:

1. It should be bimodal with a positive and a negative lobe, each of which approximates a Dirac delta function as closely as possible at predesignated pressure levels t_1 and t_2.
2. The two lobes should each have unit area, but the areas should be of opposite sign, and the crossover point should be at $t_c = (t_1+t_2)/2$.

The first property is realized by minimizing the quadratic form

$$Q(\vec{c}) = \int_{t_T}^{t_s} (t-t_1)^2(t-t_2)^2[D(\vec{c},t)-\delta(t-t_1)+\delta(t-t_2)]^2 dt$$

$$= \int_{t_T}^{t_s} (t-t_1)^2(t-t_2)^2 D^2(\vec{c},t)\, dt \qquad (18)$$

with respect to the vector $\vec{c}$. The factors $(t-t_1)^2$ and $(t-t_2)^2$ in (18) are introduced to play the role of penalty functions. They are penalty functions because they cause Q to grow rapidly in magnitude if the squared quantity in brackets deviates substantially from zero away from the points t_1 and t_2. Thus, Q is penalized least if D is a maximum in the vicinity of t_1 and t_2 and a minimum elsewhere. The second property listed above translates into the two constraints

$$\int_{t_T}^{t_c} D(\vec{c},t)\, dt = -\int_{t_c}^{t_s} D(\vec{c},t)\, dt = 1 \qquad (19)$$

and

$$D(\vec{c},t_c) = 0, \qquad (20)$$

with $t_c = (t_1+t_2)/2$.

We now wish to determine the vector $\vec{c}$ by minimizing the quadratic form (18), subject to the constraints (19) and (20). This is a classical problem that is readily solved by introducing a pair of Lagrangian multipliers λ and μ and combining Eqs. (18), (19) and (20) into a single expression, defined by $\hat{Q}$, that must be minimized, where

$$\hat{Q}(\vec{c}) = \vec{c}^T S\vec{c} + \lambda(\vec{c}^T\vec{a}-1) + \mu(\vec{c}^T\vec{b}). \tag{21}$$

The elements of the matrix S and the vectors $\vec{a}$ and $\vec{b}$ are, by (17), (18), (19) and (20), respectively,

$$S_{ij} = \int_{t_T}^{t_s} (t-t_1)^2(t-t_2)^2 \frac{dK_i(t)}{dt}\frac{dK_j(t)}{dt}\,dt, \tag{22}$$

$$a_i = \int_{t_T}^{t_c} \frac{dK_i(t)}{dt}\,dt = -\int_{t_c}^{t_s} \frac{dK_i(t)}{dt}\,dt = K_i(t_c), \tag{23}$$

and

$$b_i = \frac{dK_i(t_c)}{dt} \tag{24}$$

for i,j=1,...,n. The coefficient vector $\vec{c}$ which minimizes expression (21) satisfies the normal equation

$$\frac{d\hat{Q}}{d\vec{c}} = 2S\vec{c} + \lambda\vec{a} + \mu\vec{b} = \vec{0},$$

or

$$\vec{c} = -\frac{1}{2}S^{-1}(\lambda\vec{a} + \mu\vec{b}). \tag{25}$$

Multiplying $\vec{c}^T$ by $\vec{a}$ and $\vec{b}$, one satisfies constraints (19) and (20), that is,

$$\vec{c}^T\vec{a} = -\frac{1}{2}(\lambda\vec{a}^T + \mu\vec{b}^T)\, S^{-1}\vec{a} = 1 \tag{26}$$

and

$$\vec{c}^T\vec{b} = -\frac{1}{2}(\lambda\vec{a}^T + \mu\vec{b}^T)\, S^{-1}\vec{b} = 0. \tag{27}$$

If one sets

$$\alpha = -\frac{1}{2}\vec{a}^T S^{-1}\vec{a},\ \beta = -\frac{1}{2}\vec{a}^T S^{-1}\vec{b} = -\frac{1}{2}\vec{b}^T S^{-1}\vec{a},\ \gamma = -\frac{1}{2}\vec{b}^T S^{-1}\vec{b}, \tag{28}$$

then (26) and (27) reduce to the pair of simultaneous equations

$$\alpha\lambda - \beta\mu = 1$$

$$\beta\lambda + \gamma\mu = 0,$$

whose solutions are

$$\lambda = \frac{-\gamma}{\beta^2 - \alpha\gamma} \quad \text{and} \quad \mu = \frac{\beta}{\beta^2 - \alpha\gamma}, \tag{29}$$

provided $\beta^2 - \alpha\gamma \neq 0$. Substitution of (28) into (29), and in turn (29) into (25), yields the required coefficient vector $\vec{c}$.

We will now have to digress somewhat because when the calculations of Eqs. (22) through (29) were performed with real data disaster struck quickly. The difficulty was not with the theory, but with an unexpected practical matter, namely, the system of equations (26) and (27) was singular. In other words, $\beta^2 - \alpha\gamma = 0$ in solution (29), or nearly so. The reason this happened was that for most of the cases tried, the zero crossover naturally fell at the point $(t_1+t_2)/2$, without having to stipulate it as such through

Eq. (20). Hence, the constraint (20) was redundant with what was already an accomplished fact and the system became singular. To rectify the situation it is necessary to delete constraint (20), which resulted in the following changes. (The cases in which the system was not singular will be discussed later.)

First expression (21) takes the form

$$\hat{Q}(\vec{c}) = \vec{c}^{T} S^{-1} \vec{c} + \lambda(\vec{c}^{T}\vec{a} - 1), \tag{30}$$

which when minimized has the solution

$$\vec{c} = -\frac{\lambda}{2} S^{-1}\vec{a} \tag{31}$$

[see (25)], so that

$$\vec{c}^{T}\vec{a} = -\frac{\lambda}{2} \vec{a}^{T} S^{-1}\vec{a} = 1 \tag{32}$$

by (19), that is,

$$\vec{c} = \frac{S^{-1}\vec{a}}{\vec{a}^{T} S^{-1}\vec{a}}, \tag{33}$$

which is the required coefficient vector.

If the coefficients obtained from Eq. (33) are now used in Eq. (17), an explicit expression for the averaging kernel D is obtained. An example of such a curve is plotted as the dashed curve in Fig. 1 for which n = 4. The curve D_2 was chosen particularly because its negative lobe best coincides with the negative lobe of the solid curve labeled D_1. Recall that D_1, which was described previously, is based on a single kernel function. In order to make the proper geometric comparison between curves D_1 and D_2, they each had to be normalized by dividing the original functions by the maximum of their absolute values.

Two important facts emerge when comparing the single channel approach, as exemplified by curve D_1, with the multichannel approach, as illustrated by curve D_2. First, both lobes of D_2 are much narrower than those of D_1; hence, the mean-value assumption required to obtain Eq. (11) is more realizable for the multichannel case. Second, the levels at which the positive and negative lobes of D_2 peak are much closer together than they are for the two lobes of D_1. This permits the wind vector difference $\vec{V}(t_1) - \vec{V}(t_2)$ in (11) to be calculated more accurately.

When Eq. (16) and the bimodal averaging kernel (17) are used in place of Eq. (10), one obtains the new result

$$\sum_{i=1}^{n} c_i \vec{r}_i = -\alpha \vec{k} \times \left\{ \int_{t_T}^{t_c} \vec{V}(t) D(\vec{c},t)\,dt - \int_{t_c}^{t_s} \vec{V}(t) \left| D(\vec{c},t) \right| dt \right\}, \tag{34}$$

and then Eq. (11) takes on the form

$$\sum_{i=1}^{n} c_i \vec{r}_i = -\alpha \vec{k} \times [\vec{V}(t_1) - \vec{V}(t_2)] = -\alpha \vec{k} \times \delta\vec{V}. \tag{35}$$

The required geostrophic wind components now have the more accurate form

$$u(t_1) = u(t_2) - \frac{1}{\alpha} \sum_{i=1}^{n} c_i \left(\frac{\partial R_i}{\partial y}\right)_p \tag{36}$$

and

$$v(t_1) = v(t_2) + \frac{1}{\alpha} \sum_{i=1}^{n} c_i \left(\frac{\partial R_i}{\partial x}\right)_p. \tag{37}$$

As before, the wind components at level t_1 are inferred from those given at level t_2 and from the components of the radiance gradients, but now there is a linear combination of radiance gradients in place of a single gradient component.

4. BEST LAYERS FOR OPERATIONAL SOUNDERS

Of course the purpose in deriving Eqs. (36) and (37) is to apply these results to actual satellite data. More is said on this subject subsequently, but in this section we wish to take advantage of the diagnostic tools afforded by the averaging kernel technique. Since the levels t_1 and t_2 at which the bimodal averaging kernel lobes peak are specified by the user, averaging kernels can be calculated for all possible combinations of pairs of levels out of a given finite set of levels $\{t_k\}$. From this collection of calculations one can determine the layers over which the thermal winds can be optimally derived. The outcome depends on the particular sounding instrument being used, that is, on the shapes and numbers of kernel functions that are available.

Optimum layers were determined for the two currently operational sounders, namely, the DMSP-SSH sounder and the NOAA-TOVS sounder. The SSH has six channels in the 15-μm CO_2 absorption band that can be used for temperature sounding, but since two of these channels sense the ground, only 4 channels can be used to derive vertical wind shear. They are centered at 668.5, 677, 695, and 708 cm^{-1}. On the other hand, the TOVS sounder contains three separate instrument packages: (1) the High Resolution Infrared Radiation Sounder Number 2 (HIRS/2) with 20 channels primarily in the infrared region of the spectrum, (2) the Microwave Sounding Unit (MSU) with 4 channels in the 5.5-mm oxygen complex, and (3) the Stratospheric Sounding Unit (SSU)

with 3 channels that employ a selective absorption technique in the 15-μm CO_2 band to sound the middle stratosphere.

Two separate tests were conducted. The first test used only the four most absorbing SSH channels in Eq. (17) to obtain the bimodal averaging kernels. In order to determine the optimum pressure interval over which to calculate the wind shear, averaging kernels for 45 different combinations of pressure levels t_1 and t_2 were computed. There was no need to calculate averaging kernels for additional combinations of pressure levels because the results from neighboring levels changed by only small amounts and in a predictable manner. A search was made of the 45 calculated averaging kernels for the best ones. The criterion of "best" is those that have the narrowest main lobes while at the same time have minimal side lobes. After the search was completed two cases were found to be superior to all the others in satisfying the criterion of "best". The averaging kernels of these two cases are shown in Fig. 2 and are labeled D_3 and D_4; they also were normalized as before for comparative purposes. One concludes from these two curves that the best pressure intervals are from 12 to 125 mb and from 80 to 400 mb.

Expression (6) for the kernel functions indicates a temperature dependence; therefore, kernel functions were calculated for 9 very different U.S. Standard Atmosphere Supplements (1966). However, the same two pairs of layers that were just given were found to be best in each case. Although the averaging kernels for a fixed pair of levels t_1 and t_2 differed in shape for the 9 temperature profiles studied, the differences were only in the fine structure - the basic shape remained the same. (The averaging kernels shown in Fig. 2 are for the 45°N-July Supplementary Atmosphere.) Of course, the reason for this is that the basic shape of the kernel function given by (6) is dictated by the weighting function $d\tau_\nu(t)/dt$.

The second test used a total of 11 channels from the TOVS instrument in Eq. (17) to obtain the bimodal averaging kernels. None of the MSU channels were used in this test because the field of view is much larger than that of the HIRS/2 instrument and, therefore, could affect the accuracy of the horizontal radiance gradients, relative to those for the other instruments. The SSU also has a larger field of view than that of the HIRS/2 instrument, but because the stratosphere is believed to be more horizontally homogeneous than the troposphere is, the three SSU channels were used along with 8 of the most opaque of the HIRS/2 channels. The HIRS/2 channels used were centered at 668.5, 680, 690, 703, 716, 2240, 2270, and 2360 cm^{-1}.

The same 45 pairs of levels t_1 and t_2 as were used before were used in calculating the bimodal averaging kernels for the 11 TOVS channels. This time the search for best levels lead to three cases which are shown in Fig. 3 as curves D_5, D_6 and D_7, which were normalized as before for comparative purposes. These 3 curves are more "wiggly" than those shown in Fig. 2 for two reasons: (1) they are based on a midlatitudinal temperature profile that had more fine structure than the supplemental temperature profile used for Fig. 2, and (2) as the number of kernel functions used in the linear combination (17) is increased, more structure is possible in the resulting averaging kernel. Calculations of averaging kernels were also made for a tropical and a polar temperature profile for the 11 channels, but again the averaging kernels were sufficiently similar to those plotted in Fig. 3 that the conclusions about the best levels remain the same.

The conclusions to be drawn from Fig. 3 are that the best pressure intervals for the TOVS sounder (minus the microwave channels) are from 25 to 150 mb, from 80 to 325 mb, and from 250 to 625 mb. As would be expected,

the main lobes are narrower for the 11-channel averaging kernels of Fig. 3 than they are for the 4-channel kernels of Fig. 2. Averaging kernels were also calculated for only the 8 HIRS/2 channels. The same three pressure intervals were optimal, but the narrowness of the main lobes and size of the side lobes were degraded in a predictable way, that is, curve D_5 was degraded the most, curve D_6 was affected only slightly, and curve D_7 was virtually unaffected.

There is a caveat in what has been discussed in this section in that there should be one more best result in Fig. 2 and two more in Fig. 3. They were lost when Eqs. (21), (25), (26), (27), and (29) were replaced by Eqs. (30, (31), (32), and (33). As stated earlier, these replacements were made because in the vast majority of cases the system of equations (26) and (27) became singular. However, in the cases for which this was not true, valid results were obtained. However, at the time the singular matrices were found the computer program was thought to be faulty and the printout was thrown away. In retrospect it is clear that there were cases where the zero crossover did not occur at the level $(t_1+t_2)/2$. In these cases the calculated results with the two constraints left intact were valid. However, rather than advocate an approach where two different programs must be run to get one set of results, the author would like to present an alternative, but mathematically equivalent, single approach that yields the complete set of optimal averaging kernels.

5. AN ALTERNATIVE APPROACH

Recall that in Section 2 it was stated that one can work with either Eq. (8) or Eq. (9), and that Zak and Panofsky (1968) used Eq. (9). In the alternative approach developed in this section we begin with Eq. (8), that is,

$$\vec{r}_i = \nabla_p R_i = \alpha \vec{k} \times \int_{t_T}^{t_s} \frac{\partial \vec{V}}{\partial t} K_i(t)\, dt, \qquad i=1,\ldots,n. \tag{38}$$

The intent here is again to use a modified Backus-Gilbert method to produce optimal averaging kernels, but because the derived quantity in (38) is vertical wind shear instead of the geostrophic wind vector, different optimization criteria are required.

Following the development in Section 3, one multiplies each of the n equations in (38) by an undetermined coefficient c_i and then sums the resulting n equations to obtain the single equation:

$$\sum_{i=1}^{n} c_i \vec{r}_i = \alpha \vec{k} \times \int_{t_T}^{t_s} \frac{\partial \vec{V}}{\partial t} \left[\sum_{i=1}^{n} c_i K_i(t) \right] dt. \tag{39}$$

The quantity in square brackets, though different from that of Eq. (16), is again an averaging kernel which will be denoted by R, that is,

$$R(\vec{c},t) = \sum_{i=1}^{n} c_i K_i(t). \tag{40}$$

This time the choice of coefficients has a different motivation. We are interested in determining the average wind shear between levels t_1 and t_2, that is,

$$\left\langle \frac{\partial \vec{V}}{\partial t} \right\rangle = \frac{1}{t_2 - t_1} \int_{t_1}^{t_2} \frac{\partial \vec{V}}{\partial t}\, dt. \tag{41}$$

Therefore, if in Eq. (39) the averaging kernel were a rectangular unit function defined by

$$\rho(t;t_1,t_2) = \left\{ \begin{array}{ll} 1 & \text{for } t_1 \leq t \leq t_2 \\ 0 & \text{otherwise} \end{array} \right\}, \qquad (42)$$

then the mean value theorem applied to Eq. (39) would yield the average wind shear defined by (41).

As a consequence of the foregoing the averaging kernel (40) should have the following properties:

1. It should approximate the rectangular unit function ρ, as defined by (42), as closely as possible for predesignated pressure levels t_1 and t_2.
2. The nonzero portion of the averaging kernel (i.e., between t_1 and t_2) should have a uniform height of unity.

The first property is realized by minimizing the quadratic form

$$Q(\vec{c}) = \int_{t_T}^{t_s} [1-\rho(t;t_1,t_2)]^2 \, [R(\vec{c},t) - \rho(t;t_1,t_2)]^2 \, dt$$

$$= \int_{t_T}^{t_1} R^2(\vec{c},t)dt + \int_{t_2}^{t_s} R^2(\vec{c},t)dt \qquad (43)$$

with respect to the vector $\vec{c}$. The factor $[1-\rho]^2$ is a penalty function. The second line of Eq. (43) says that the portion of the averaging kernel outside the rectangle should have a minimum value. The second property listed above cannot be put into a form that can be manipulated analytically. However, a partial solution to this difficulty is provided by the constraint that the averaging kernel between t_1 and t_2 have an average height of unity, that is,

that

$$\frac{1}{t_2-t_1}\int_{t_1}^{t_2} R(\vec{c},t)dt = 1. \tag{44}$$

The determination of the vector $\vec{c}$ by minimizing the quadratic form (43), subject to the constraint (44), is again the problem given by Eqs. (30), (31), and (32), whose solution is given by

$$\vec{c} = \frac{S^{-1}\vec{a}}{\vec{a}^T S^{-1}\vec{a}}, \tag{45}$$

which is Eq. (33), except that the elements of the matrix S and the vector $\vec{a}$ are different. In this case, by Eqs. (40, (43), and (44), the respective elements are given by:

$$S_{ij} = \int_{t_T}^{t_1} K_i(t)\, K_j(t)dt + \int_{t_2}^{t_s} K_i(t)\, K_j(t)dt \tag{46}$$

and

$$a_i = \frac{1}{t_2-t_1}\int_{t_1}^{t_2} K_i(t)dt, \tag{47}$$

for i,j=1,...,n. The vector $\vec{c}$ given by (45) is the required coefficient vector, which when applied to Eq. (40) provides the best approximation to a rectangular unit function by the averaging kernel.

When (40) is applied to (39) and the second mean-value theorem for integrals is applied, one has

$$\sum_{i=1}^{n} c_i \vec{r}_i = \alpha \vec{k} \times \langle \frac{\partial \vec{V}}{\partial t} \rangle \int_{t_T}^{t_s} R(\vec{c},t)dt$$

$$= \alpha \hat{k} \times \langle \frac{\partial \vec{V}}{\partial t} \rangle (t_2 - t_1) . \qquad (48)$$

But by the law of the mean for derivatives

$$\frac{\vec{V}(t_2) - \vec{V}(t_1)}{t_2 - t_1} = \langle \frac{\partial \vec{V}}{\partial t} \rangle , \qquad (49)$$

so that the required geostrophic wind components by (48) have the form

$$u(t_1) = u(t_2) + \langle \frac{\partial u}{\partial t} \rangle (t_2 - t_1) = u(t_2) + \frac{1}{\alpha} \sum_{i=1}^{n} c_i \left(\frac{\partial R_i}{\partial y}\right)_p , \qquad (50)$$

and

$$v(t_1) = v(t_2) + \langle \frac{\partial v}{\partial t} \rangle (t_2 - t_1) = v(t_2) - \frac{1}{\alpha} \sum_{i=1}^{n} c_i \left(\frac{\partial R_i}{\partial x}\right)_p . \qquad (51)$$

The interpretation of Eqs. (50) and (51) is (as before) that the wind components at level t_1 are inferred from those given at level t_2 plus the linear combination of components of the radiance gradients. Note that, aside from a difference in sign, Eqs. (50) and (51) are identical to Eqs. (36) and (37), as they should be since the starting points, namely Eqs. (8) and (9), are just different forms of the same equation. However, this numerical exercise has produced a large gain in that all optimal pressure intervals are found at one time as the solution to the problem given by Eqs. (45), (46), and (47).

6. RESULTS

The two tests described in Section 4 were also applied to the rectangular averaging kernels of Eq. (40). All details and conclusions of the tests in Section 4 remain the same, including the kinds and numbers of channels used, the temperature dependence of the kernel functions, and the combinations of pressure levels that were computed.

In the first test three averaging kernels (one more than in Section 4) were found to satisfy the criterion of "best", and are shown in Fig. 4 with the labels R_1, R_2, and R_3. They do not have "rectangular" shapes because the kernel functions used in the linear combination (40) are all rounded in the manner of the curves shown in Fig. 4. The three curves in Fig. 4 indicate that the best pressure intervals (t_1,t_2) for the DMSP sounder are: 10 to 125 mb, 80-400 mb, and 300-750 mb. For the second test the best rectangular averaging kernels for the TOVS sounders are shown in Fig. 5. These five curves (two more than in Section 4) yield best pressure intervals of: 35-150, 115-330, 175-500, 285-625, and 400-875 mb.

A comparison of the unimodal curves in Fig. 4 with those in Fig. 5 clearly shows the lobes of Fig. 5 to be narrower than those of Fig. 4, with the important consequence that the sides of the lobes in Fig. 5 drop more vertically than they do in Fig. 4. Again, this is to be expected because the additional channels that are used to produce the averaging kernels in Fig. 5 give more flexibility to the shape of the averaging kernels. Also, when 8 HIRS/2 channels were used in place of the original 11 channels, the conclusions are as before, that is, curve R_4 is most strongly effected, curve R_5 is effected only slightly, and curves R_6, R_7, and R_8 are virtually unaffected.

The conclusions of Sections 4 and 6 as to which pressure intervals are best are conveniently summarized in Table 1. The additional channels on the TIROS-N satellite provided more layer options than were available from

Table 1. Best layers over which to calculate the average vertical wind shear, based on the SSH and TOVS sounders, for the bimodal and unimodal averaging kernels.

	Bimodal Averaging Kernel	Unimodal Averaging Kernel
SSH	12-125 mb	10-125 mb
Sounder	80-400 mb	80-400 mb
	*	300-750 mb
	25-150 mb	35-150 mb
TOVS	80-325 mb	115-330 mb
Sounder	*	175-500 mb
	250-625 mb	285-625 mb
	*	400-875 mb

*Missing because only the results from the single-constraint problem are available (see the dicussion at the end of Section 4).

the DMSP satellite. Note the similarity between adjacent entries in the two columns. The slight differences in pressure intervals can be attributed to differences in the numerical procedures used to calculate the averaging kernels.

7. METHODS FOR DERIVING WINDS

Now that the diagnostic studies have been completed, we can discuss the main issue, namely, how can one derive winds at one pressure level,

given the winds at a second level plus the gradients of the radiances. One method has been discussed in Sections 3 and 5, but other methods are also possible. Brief discussions of three distinct methods are now presented.

A. Averaging Kernels

The most obvious method to use is the one described in Sections 3 and 5. In short, one prescribes pressure levels t_1 and t_2 and then uses Eqs. (36) and (37), or equivalently, Eqs. (50) and (51). However, when these equations are applied to real data, the noise in the measured radiances must be taken into account. A solution to this problem is given by Backus and Gilbert (1970). Briefly, one must either derive a covariance matrix E for the measurement error, or model one from certain assumptions about the behavior of the noise. Then the variance of the solution due to the random errors of measurement is of the form

$$\sigma^2(\vec{c}) = \vec{c}^T E \vec{c}. \tag{52}$$

Now instead of minimizing quadratic form (18) or (43), one must minimize the linear combination of quadratic forms

$$qQ(\vec{c}) + (1-q)\,\sigma^2(\vec{c}), \tag{53}$$

where $0 \leq q \leq 1$. Expression (53) must also be subject to the proper constraints, which can be (19) and (20); or just (19); or just (44). The choice of the value for the scalar q depends upon the tradeoff arrangement one wants between minimizing noise and the accuracy of the shape of the averaging kernel. The tradeoff decision depends in turn upon the particular application at hand. The best pressure levels to apply to this method are listed in Table 1.

This method should be used with real data only if the following two assumptions apply:

1. One requires only geostrophic winds, not the true winds, and
2. The transmittance functions of the radiative transfer equation are known with reasonable accuracy.

B. Vertical Profile Retrievals

One really need not go any further than Eq. (8) or (9). Since both of these equations require quantities that are known and available, namely, well-defined kernel functions and n vectors of $\nabla_p R_i$, one can retrieve vertical profiles of the wind shear from Eq. (8) or vertical profiles of the geostrophic wind vector from Eq. (9). These kinds of retrieval methods are described in a paper by Fleming and Smith (1967), and are applicable because Eqs. (8) and (9) are linear Fredholm integral equations of the first kind.

When Eq. (9) is used, the wind profile is available directly, but since it will be accurate in only a relative sense, one should take the difference $\delta\vec{V}$ between the wind vector profile at levels t_1 and t_2 and apply this difference to the first parts of Eqs. (13) and (14), provided the wind components $u(t_2)$ and $v(t_2)$ are known.

If Eq. (8) is used, then the retrieved vertical wind shear profile is applied to Eq. (41) to determine the average wind shear $\left\langle \frac{\partial \vec{V}}{\partial t} \right\rangle$ between levels t_1 and t_2. This average value is then applied to the first parts of Eqs. (50) and (51), provided the wind components $u(t_2)$ and $v(t_2)$ are known. Again, the best levels at which to apply this method are listed in Table 1. The same two assumptions that were listed under Method A above apply here as well, except that since this is an inverse method, the transmittance functions of the radiative transfer equation must be known with even greater accuracy than that required for Method A.

C. Regression

When true winds are required (as opposed to thermal winds), one of the most appropriate methods is ordinary regression in which the radiance gradients are used as the predictors. To carry out this procedure, one needs to compile a large sample of true wind data which are coincident in time and place with satellite radiance measurements from which horizontal gradients can be calculated. The necessary regression coefficient matrix can then be computed from matrices of these coincident measurements. This method is standard, and so details will not be given here. One can find specifics in the paper by Fleming and Smith (1967). The best layers given in Table 1 apply to the regression method as well because those layers are the very ones over which the radiance gradients are the most sensitive as predictors.

8. CONCLUSIONS

The final shapes of the averaging kernels in Figs. 2 through 5 are not ideal. One reason for this is that there are too few kernel functions to work with, but a far more important reason is that one cannot dictate the shapes of the individual kernel functions because they are prescribed by the physical properties of the atmosphere. Consequently, they are not even linearly independent (that is, relative to the noise level of the measurements), and, therefore, are not very effective basis functions.

The use of the words "optimum" and "best" in this report needs clarification. For a given set of pressure levels t_1 and t_2 the corresponding averaging kernel is optimum in that it minimizes the defining quadratic form. Thus, there is one optimum averaging kernel for each pair of given pressure levels. But then out of all of these optimum averaging kernels

the best ones were chosen to be the ones which had the truest main lobe shape and the smallest side lobe amplitude.

Even though several methods for calculating winds were presented, the regression approach to obtaining true winds should be the most useful approach. In pursuing this approach several recommendations can be made that result directly from this study:

1. As many channels as possible should be used as predictors, even though a particular kernel function may contribute only weakly to the level of the atmosphere in question.
2. Winds cannot be inferred with equal accuracy at all levels of the atmosphere. Since the preliminary work of deciding which pressure levels yield the most accurate winds has been done in this report (when radiance gradients are used as predictors), one need only refer to Table 1 to decide on the pressure levels at which to collect wind data.
3. The diagnostic tools developed in this report are useful in helping to answer questions about the sensitivity of the solution to a given channel or about the results that can be expected if an instrument other than the SSH or TOVS sounders is used (e.g., a microwave sounder).

REFERENCES

Backus, G. E., and J. F. Gilbert, 1970: Uniqueness in the inversion of inaccurate gross earth data. Phil. Trans. Roy. Soc. London, A266, 123-192.

Conrath, B. J., 1972: Vertical resolution of temperature profiles obtained from remote radiation measurements. J. Atmos. Sci., 29, 1262-1271.

Fleming, H. E., and W. L. Smith, 1972: Inversion techniques for remote sensing of atmospheric temperature profiles. In Temperature: Its Measurement and Control in Science and Industry. Edited by H. H. Plumb, Instrument Society of America, Pittsburgh, Vol. 4, Part 3, pp. 2239-2250.

Grody, N. C., C. M. Hayden, W.C.C. Shen, P. W. Rosenkranz, and D. H. Staelin, 1979: Typhoon June winds estimated from scanning microwave spectrometer measurements at 55.45 GHz. J. Geophys. Res., 84, No. C7, 3689-3695.

U. S. Committee on Extension to the Standard Atmosphere (COESA), 1966: U. S. Standard Atmosphere, Supplements, 1966. U. S. Government Printing Office, Washington, D. C.

Zak, J. A., and H. A. Panofsky, 1968: Estimation of stratospheric flow from satellite 15-micron radiation. J. Appl. Meteor., 7, 136-140.

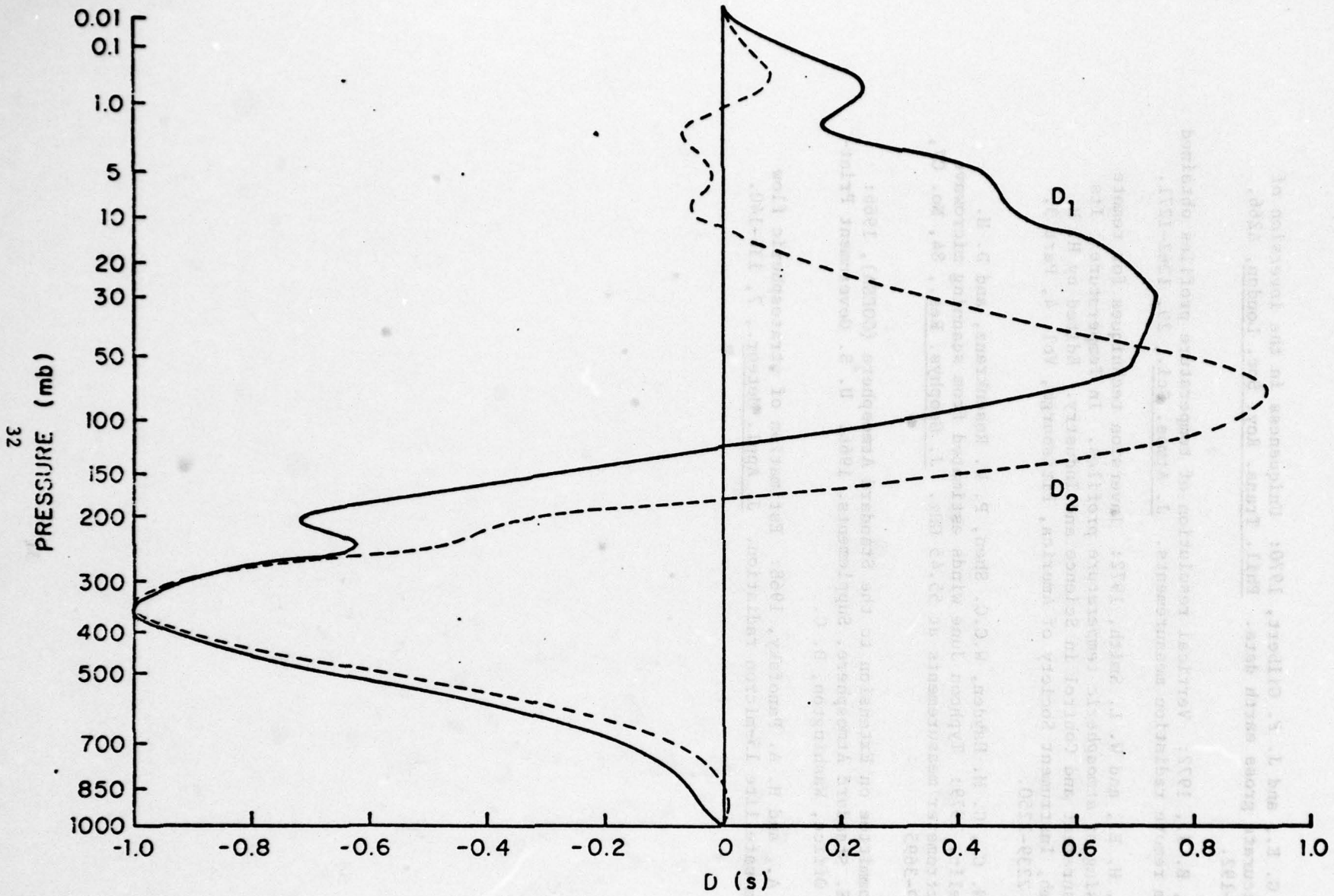

Figure 1. The normalized derivative of a single kernel function (solid curve) versus the normalized averaging kernel of four kernel function derivatives (dashed curve).

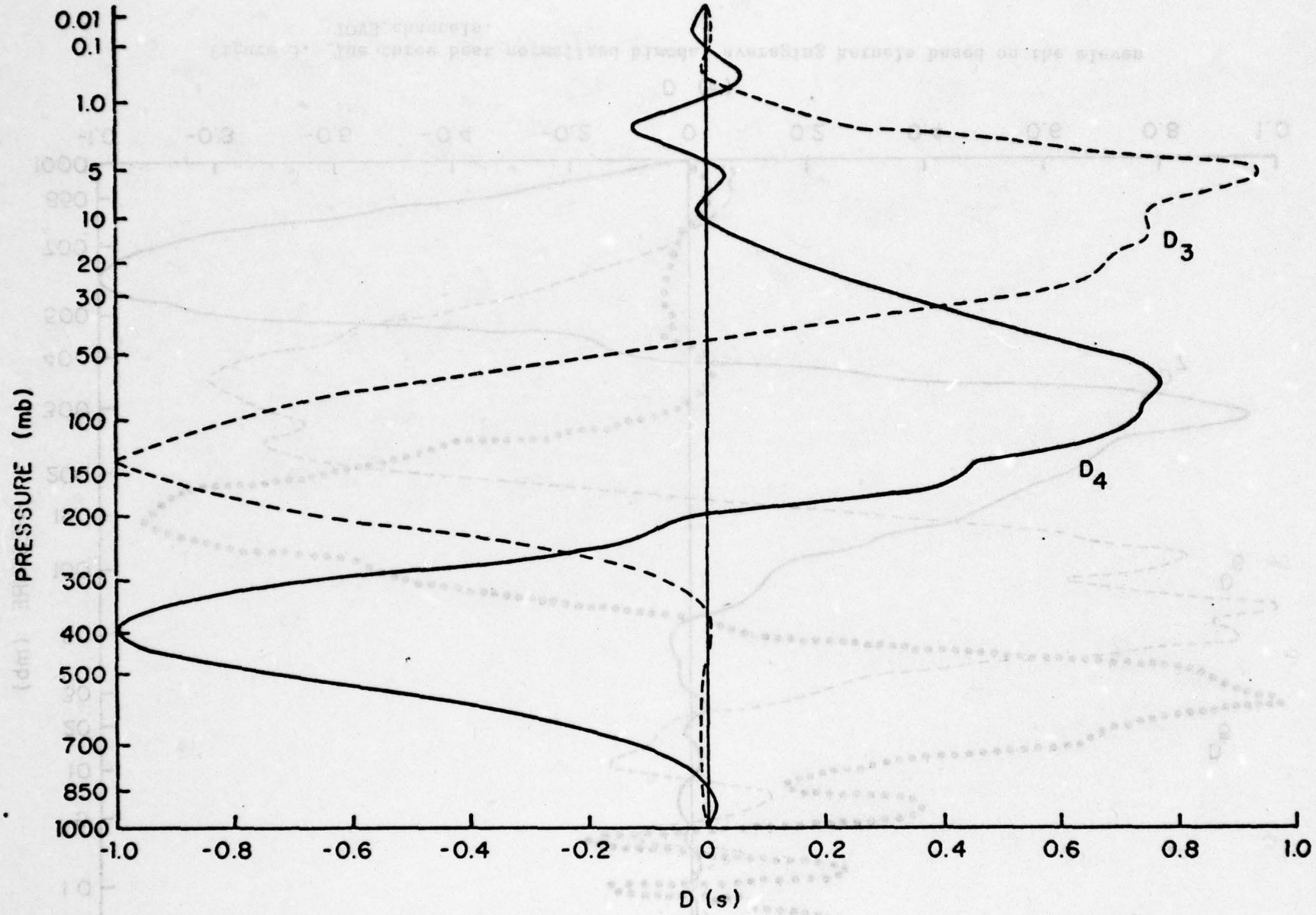

Figure 2. The two best normalized bimodal averaging kernels based on the four SSH channels.

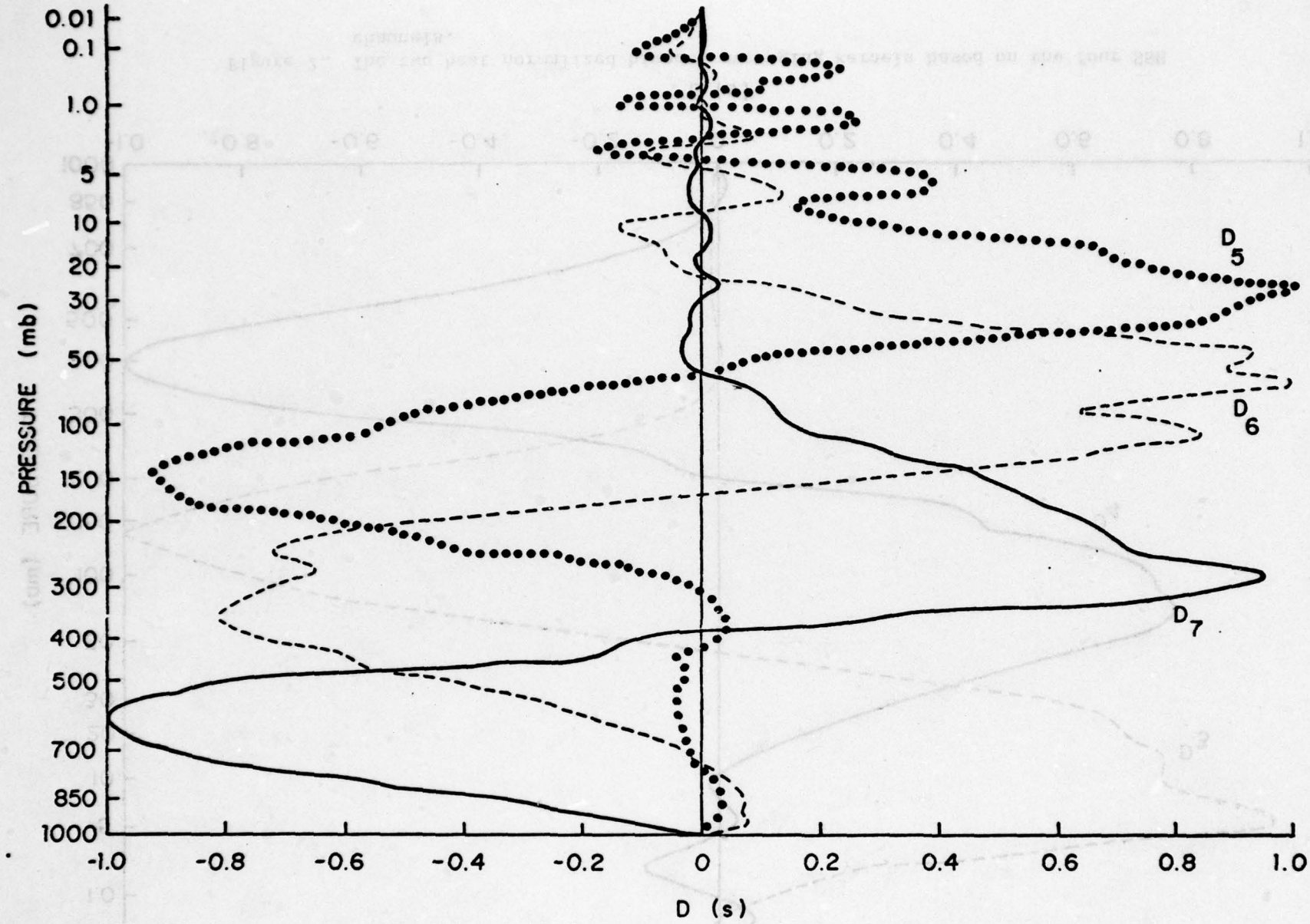

Figure 3. The three best normalized bimodal averaging kernels based on the eleven TOVS channels.

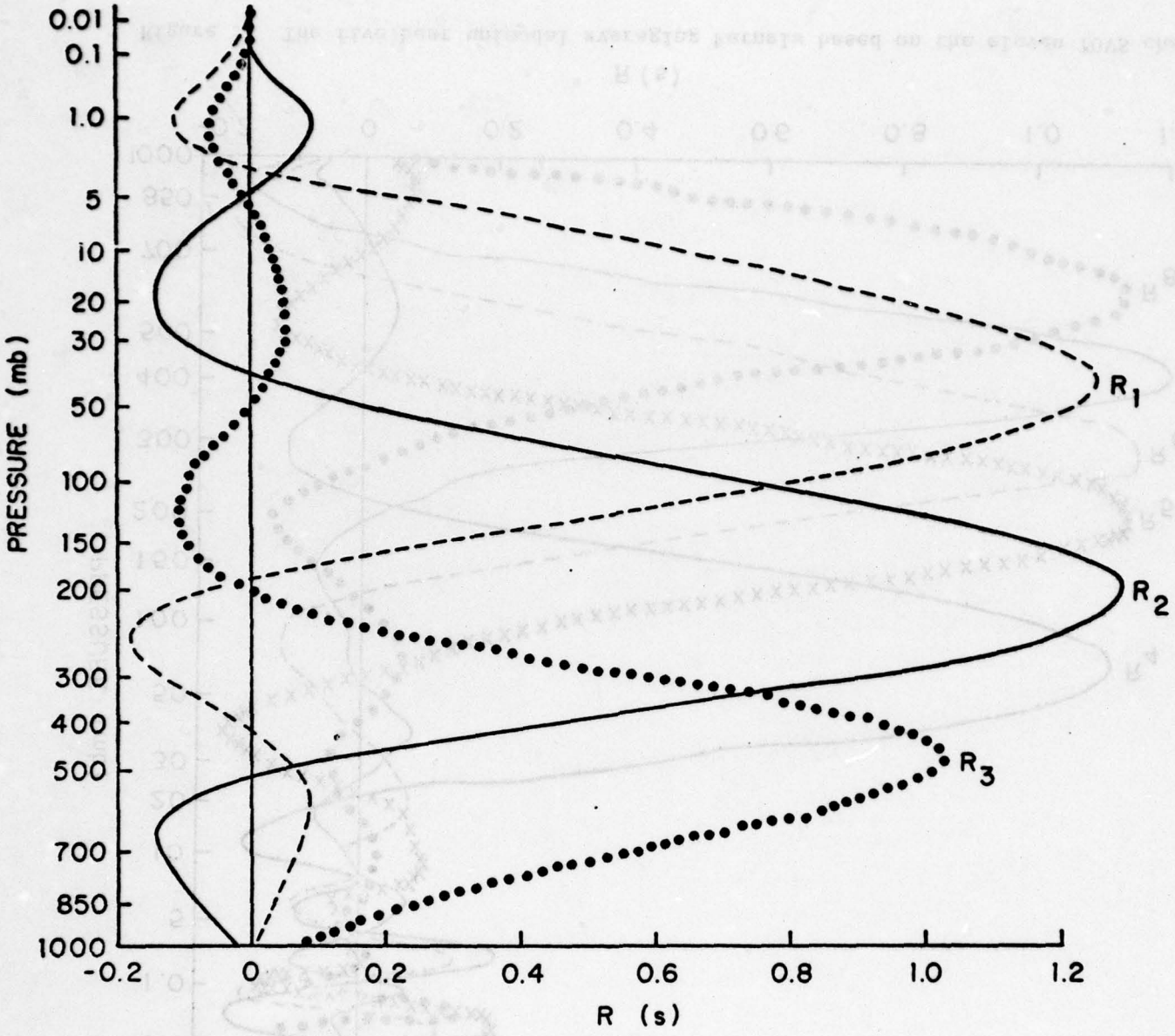

Figure 4. The three best unimodal averaging kernels based on the four SSH channels.

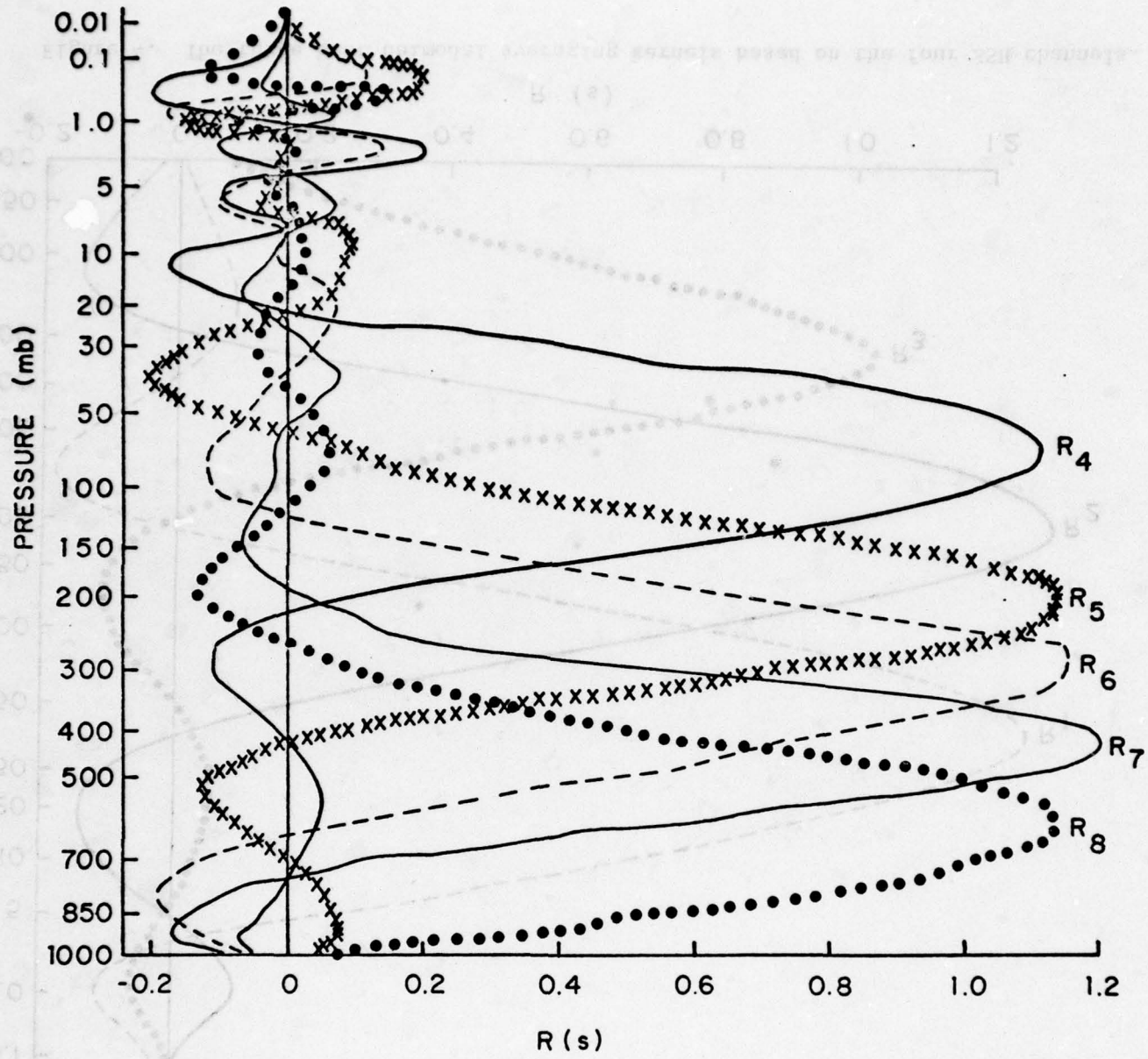

Figure 5. The five best unimodal averaging kernels based on the eleven TOVS channels.

DISTRIBUTION LIST

		No. Copies
1.	Defense Documentation Center Cameron Station Alexandria, Virginia 22314	2
2.	Library, Code 0142 Naval Postgraduate School Monterey, California 93940	2
3.	Dr. R. T. Williams, Code 63Wu Department of Meteorology Naval Postgraduate School Monterey, California 93940	1
4.	Dr. W. Van der Bijl, Code 63Vb Department of Meteorology Naval Postgraduate School Monterey, California 93940	1
5.	CDR F. R. Williams, Code 63Wf Department of Meteorology Naval Postgraduate School Monterey, California 93940	1
6.	Commander Naval Oceanography Command National Space Technology Laboratories Bay St. Louis, Mississippi 39520	1
7.	Officer in Charge Navy Environmental Prediction Research Facility Monterey, California 93940	10
8.	Dean of Research, Code 012 Naval Postgraduate School Monterey, California 93940	2
9.	Commanding Officer Fleet Numerical Weather Central Monterey, California 93940	5
10.	Naval Oceanographic Office Library, Code 3330 Washington, D. C. 20373	1
11.	AFGL Research Library L. G. Hanscom Field Bedford, Massachusetts 01730	1

12. Commander, Air Weather Service — 1
Military Airlift Command
United States Air Force
Scott Air Force Base, Illinois 62226

13. Atmospheric Sciences Library — 1
National Oceanic and Atmospheric Administration
Silver Spring, Maryland 20910

14. Dr. F. P. Bretherton — 1
National Center for Atmospheric Research
P. O. Box 3000
Boulder, Colorado 80303

15. Dr. John Brown — 1
National Meteorological Center/NOAA
World Weather Building
Washington, D. C. 20233

16. Dr. C.-P. Chang, Code 63Cp — 1
Department of Meteorology
Naval Postgraduate School
Monterey, California 93940

17. Dr. Robert J. Renard, Code 63Rd — 1
Department of Meteorology
Naval Postgraduate School
Monterey, California 93940

18. Dr. Fred Shuman, Director — 1
National Meteorological Center
World Weather Building
Washington, D. C. 20233

19. Dr. R. L. Elsberry, Code 63Es — 1
Department of Meteorology
Naval Postgraduate School
Monterey, California 93940

20. Dr. Mitsuru Sekioka — 1
Professor, Institute of Meteorology
The Defense Academy
Yokosuka, Kanagawa 239 JAPAN

21. Dr. G. J. Haltiner, Code 63Ha — 5
Chairman, Department of Meteorology
Naval Postgraduate School
Monterey, California 93940

22. Dr. R. L. Haney, Code 63Hy — 1
Department of Meteorology
Naval Postgraduate School
Monterey, California 93940

23. Meteorology Library, Code 63 — 1
Naval Postgraduate School
Monterey, California 93940

24. National Center for Atmospheric Research — 1
Box 1470
Boulder, Colorado 80302

25. Department of Oceanography, Code 68 — 1
Naval Postgraduate School
Monterey, California 93940

26. Office of Naval Research — 1
Department of the Navy
Washington, D. C. 20360

27. Dr. N. A. Phillips — 1
National Meteorological Center/NOAA
World Weather Building
Washington, D. C. 20233

28. Dr. J. Smagorinsky, Director — 2
Geophysical Fluid Dynamics Laboratory
Princeton University
Princeton, New Jersey 08540

29. CDR K. Van Sickle, USN — 1
Naval Air Systems Command 370G
Washington, D. C. 20361

30. Dr. H. A. Panofsky — 1
Department of Meteorology
The Pennsylvania State University
503 Walker Building
University Park, Pennsylvania 16802

31. Dr. John Cahir — 1
Department of Meteorology
The Pennsylvania State University
503 Walker Building
University Park, Pennsylvania 16802

32. Mr. Roland E. Nagle — 5
Navy Environmental Prediction Research Facility
Monterey, California 93940

33. Dr. William L. Smith — 2
NOAA/NESS Mesoscale Applications Branch
Space Science and Engineering Center
1225 W. Dayton Street
Madison, Wisconsin 53706

34. Dr. Albert Arking 1
National Aeronautics and Space Administration
Goddard Space Flight Center
Code 911, Bldg 22, Room 322
Greenbelt, Maryland 20771

35. Mr. Lawrence Breaker 1
Satellite Field Services Station
NOAA/NESS
660 Price Avenue
Redwood City, California 94063

36. W. R. Bandeen, Code 910 1
National Aeronautics and Space Administration
Goddard Space Flight Center
Greenbelt, Maryland 20771

37. Dr. Barney J. Conrath 1
National Aeronautics and Space Administration
Goddard Space Flight Center
Bldg 21, Code 622
Greenbelt, Maryland 20771

38. Dr. Douglas Depriest 1
Office of Naval Research (Code 436)
800 N. Quincy Street
Arlington, Virginia 22217

39. Dr. Adarsh Deepak 1
Institute for Atmospheric Optics and
Remote Sensing
Post Office Box P
Hampton, Virginia 23666

40. Dr. K. L. Davidson, Code 63Ds 1
Department of Meteorology
Naval Postgraduate School
Monterey, California 93940

41. Prof. Roland S. Drayson 1
Research Activities Bldg.
University of Michigan
Ann Arbor, Michigan 48105

42. Mrs. Catherine Frain 1
S311, Rm 711B Stop G
World Weather Building
Washington, D. C. 20233

43. Prof. Sigmund Fritz 1
Graduate Program in Meteorology
2207 Space Sciences Bldg.
University of Maryland
College Park, Maryland 20742

44. Dr. Warren Hovis — 1
Director, Satellite Experiment Laboratory
NOAA/NESS, S32
Federal Building No. 4
Suitland, Maryland 20233

45. Dr. Alain L. Fymat — 1
Mail Stop 183B-365
Jet Propulsion Laboratory
4800 Oak Grove Drive
Pasadena, California 91103

46. C. M. Hayden — 1
NESS/UW
1225 West Dayton Street
Madison, Wisconsin 53706

47. Dr. Larry M. McMillin — 1
NOAA/NESS
S321, Mail Stop B
Federal Building No. 4
Suitland, Maryland 20233

48. Dr. Frank L. Martin, Code 63 — 1
Department of Meteorology
Naval Postgraduate School
Monterey, California 93940

49. Dr. Robert McClatchey — 1
Air Force Geophysics Laboratory
ATTN: OPI
L. G. Hanscom Air Force Base
Bedford, Massachusetts 01730

50. Prof. George Ohring — 1
Tel-Aviv University
Department of Geophysics and Planetary Sciences
Ramat-Aviv, Tel-Aviv, ISRAEL

51. Mr. Walter Planet — 1
NOAA/NESS
S321, Mail Stop B
Federal Building No. 4
Suitland, Maryland 20233

52. Prof. Owen Thompson — 1
Meteorology Group, Room 2213
Space Science Building
College Park, Maryland 20742

53. Dr. David Q. Wark — 1
Route S3, Mail Stop-B, NOAA/NESS
Federal Building No. 4, Room 0215
Suitland, Maryland 20233

54. Dr. Michael Weinreb 1
NOAA/NESS S321B
Federal Building No. 4
Suitland, Maryland 20233

55. Mr. Harold Yates 1
Director, Office of Research
NOAA/NESS, S2
Federal Building No. 4
Suitland, Maryland 20233

56. Henry E. Fleming 25
NOAA/NESS S321-B
Federal Building No. 4
Suitland, Maryland 20233

57. Dr. Edward B. Westwater 1
Environmental Radiometry R45x4
Wave Propagation Laboratory
Environmental Research Labs
Boulder, Colorado 80302

58. Dr. R. Madala 1
Code 6780
Naval Research Laboratory
Washington, D. C. 20375